Heliyon 8 (2022) e10695

Contents lists available at ScienceDirect

Heliyon

journal homepage: www.cell.com/heliyon

Research article

Effects of slag-based cementitious material on the mechanical behavior and heavy metal immobilization of mine tailings based cemented paste backfill

Fawen Zhang [a,*], Yinyue Li [a], Jinhui Zhang [a], Xin Gui [a], Xiuhong Zhu [a], Changmin Zhao [b]

[a] College of Forestry, Henan Agricultural University, Zhengzhou, China
[b] Zhengzhou Ecological and Environmental Monitoring Center, Zhengzhou, China

ARTICLE INFO

Keywords:
Cemented paste backfill
Heavy metals
Mechanical strength
Immobilization
Hydration products
Slag

ABSTRACT

Slag-based cementitious material was synthesized from blast furnace slag, clinker, gypsum, and activator to replace cement in cemented paste backfill (CPB). We researched the influence of slag-based cementitious material dosages and curing times on the properties of CPB, including unconfined compressive strength tests, leachate toxicity and chemical speciation of heavy metal as well as microstructural tests and analyses. The results indicated that the addition of slag-based cementitious material improved the compressive strength of the CPB, which attained the compressive strength requirements (≥1.0 MPa) at 28 days. The leachate concentrations of Pb, Cr, Cu, and Cd in CPB decreased as the slag-based cementitious material dosage and curing period increased, which met the standard (GB 5085.3-2007). The dosage of 10% slag-based cementitious material could effectively immobilize the heavy metals in the tailings, and the immobilization performance was similar to that of 20% cement, which indicated the amount of slag-based cementitious material was only half the quantity of cement in CPB. Microstructural analysis showed the hydration products included calcium silicate hydrate, ettringite, and portlandite, which could enhance the bonding force between the tailing grains.

1. Introduction

Mine tailings are solid waste residues generated during the exploitation of mineral resources and contain substantial quantities of heavy metal [1, 2, 3, 4]. The disposal of untreated tailings using tailing ponds not only requires large areas but also raises serious concerns regarding mine safety, the economy, and the environment [5, 6, 7]. In 2007, the Ministry of Land and Resources advanced a proposal of "green mine" construction in China [8]. The proper treatment of tailings from mining and smelting is very important. Cemented paste backfill (CPB) is a commonly used method for underground tailing management to reduce tailing discharge and support the roofs of underground stopes, as well as mitigate the geotechnical and environmental problems associated with them [9, 10, 11, 12]. CPB is a complex material composed of dehydrated mine tailings (70–85% of the total solid weight), binders (3–7% of the total solids weight), and fresh or processed water. It may be transported and placed into underground openings in any convenient consistency, which results in zero-waste production [13, 14, 15, 16, 17].

The type and quantity of the binder considerably influence the mechanical behavior and cost of CPB. Typically, ordinary Portland cement (OPC) is the most widely used cementitious material in CPB as it augments desirable mechanical behaviors. OPC, when used as the sole binder, is responsible for more than 70% of the total cost of CPB. In addition, the OPC production process is energy-intensive and associated with severe environmental pollution, resulting in huge CO_2 emissions. Several researchers point out that for every ton of OPC produced, 0.85–1.12 tons of CO_2 is emitted into the atmosphere [18, 19]. The OPC manufacturing industry is responsible for approximately 5–8% of the CO_2 emission in the world, thereby contributing considerably to the greenhouse effect [20, 21, 22].

Hence, the continued application of OPC as a binder will limit the extensive use of CPB. However, replacing it with a suitable cementitious material that can support "peak carbon dioxide emissions" and help realize "carbon neutrality" will promote the use of CPB [23]. Thus, identifying a low-carbon, low-cost binder to substitute for the OPC has become critical to decreasing the carbon emissions associated with CPB. In recent years, CPB technology has been extensively applied across the world and new kinds of cementitious materials have been developed for use with CPB. Several studies have been conducted to identify industrial solid wastes that can partially or even completely replace OPC [24, 25, 26, 27, 28, 29]. Zhang et al. [30] focused on the effect of additives (e.g., fly ash, slag, quicklime, etc.) on the rheological and mechanical

* Corresponding author.
E-mail address: zhangfawen@henau.edu.cn (F. Zhang).

https://doi.org/10.1016/j.heliyon.2022.e10695
Received 10 April 2022; Received in revised form 19 June 2022; Accepted 14 September 2022

behaviors of cemented foam backfill, and investigated the influence mechanism of the type and quantity of additives on the mechanical properties of CPB. Sun et al. [31] researched the synthesis and internal structure of fly ash geopolymer paste backfill materials, paying particular attention to the effect of density, the proportion of fine gangue, and dosage of fly ash on the mechanical performance of CPB. He et al. [32] proposed a method to increase the compressive strength of the cemented fine tailings backfill by using a composite binder based on industrial waste. Deng et al. [33] prepared a new CPB comprised of gangue rocks, fly ash, quicklime, and OPC, which could help build cleaner mines and power plants. Chen et al. [34] studied the effect of partially replacing OPC with modified granulated copper slag in CPB and studied the mechanical behavior and hydration reaction of CPB activated by two activators, namely, Na_2SO_4 and CaO. Jiang et al. [35] investigated the efficacy of slag as an alternative cementitious material by surveying the effects on the workability and mechanical behavior of CPB, to help devise more safe and eco-environmental CPB combinations. Zheng et al. [36] explored the possibility of utilizing slag as a cementitious material in CPB and indicated that the dosage of MgO had a considerable influence on the developed strength of CPB. Zheng et al. [37] considered that the utilization of slag cement could effectively strengthen the tailings with the addition of limestone. In a study conducted by Eker and Bascetin [38], it was seen that using silica fume instead of cement could not increase the mechanical strength of CPB, but also effectively prevent sulphate attacks in paste backfill mixture.

However, the tailings usually contain a large quantity of heavy metals (HMs), such as Pb, Cd, Cu, Cr, and As, and the leachate is highly polluting [39, 40]. It is essential to guarantee that the HMs that leach from the tailings satisfy existing pollution standards. CPB has been definitively identified as a useful method for the solidification of mine tailings containing HMs [41]. In previous studies, toxic leaching tests used for the environmental assessment of treated tailings have been described in detail. The rare earth tailings-based geopolymer prepared by Hu et al. [42] not only had good mechanical performance but could also solidify the HMs well. Li et al. [2] reported that the immobilization of HMs in bricks made from mine tailings was high, resulting leachate HMs concentrations that were all within the stipulated limits. Argane et al. [43] discussed the environmental behavior of mortars containing base metal tailings, which indicated that the risk of HMs release from tailings-based mortars was minor. Zhang et al. [44] researched the immobilization of high-arsenic-containing tailings by using metallurgical slag-cementing materials, which indicated that full solid waste materials could be used to create potential arsenic solidification materials. Zhang et al. [45] investigated the leaching characteristics of As in green-mining-fill samples, which revealed solidification/stabilization mechanism of As using slag-based binder. Wan et al. [46] synthesized geopolymers that could effectively immobilize Zn when the content of metakaolin was 50%, which increased the proportion of leached Zn to total Zn from 0.91 to 9.76%. Kiventerä et al. [39] reported the activation of tailings with calcium hydroxide and 10–25% of slag, which can effectively consolidate more than 99% of the As after a week of curing. Wan et al. [47] studied the immobilization speciation of Pb in alkali-activated binders in mine tailings, which resulted in leachate Pb concentrations of less than 5 ppm. However, the previous studies focused on the toxicity of the CPB leachate and ignored the influence of binder quantity and curing period on the leachability of HMs from CPB.

The above-mentioned binders generally have the disadvantages of large investment, high cost, poor strength, and complicated processing requirements, which makes the widespread application difficult. Blast-furnace slag (BFS) is a solid residue from the iron production industry, which is produced in blast furnaces as a compound of calcium silicates and aluminosilicates and generally cooled using water jets [48, 49]. BFS has long been utilized as a subsidiary substance in cement and concrete owing to its very good pozzolanic effect. Much research has been done on the composition, physical and chemical characteristics, and activity of BFS [50, 51]. In the past few decades, BFS has been commonly used to replace OPC in mine fillings, which can facilitate a reduction in the dosage of cementitious materials. Compared with OPC, BFS offers the advantages of rapid strength improvement, good durability, and resistance to chemical corrosion [36]. More importantly, the cost of BFS is only one-third of that of OPC, making it an ideal substitute for the expensive CPB binder [52]. However, the hydration process and consolidation mechanism of slag in the paste backfilling process have not been studied extensively.

The key to improving CPB performance is to identify a suitable cementitious material not only offering advantages in terms of safety and strength, but also ensuring the immobilization of HMs in the hardened CPB. This study focuses on the identification of a novel binder using BFS as the main raw material, called slag-based cementitious material, which is used to treat mine tailings in CPB. The major objective of this study is to comprehensively investigate the mechanical behavior, leachate toxicity and leachability, chemical speciation of HMs, and micro-level behavior of CPB under different slag-based cementitious material dosages and curing times. The mechanical properties of CPB were measured using an unconfined compressive strength (UCS) test. The immobilization of HMs (such as Pb, Cr, Cu, and Cd) was tested using the toxicity characteristic leaching procedure (TCLP) and the chemical speciation was identified by a modified Community Bureau of Reference (BCR) test. Besides, the microstructure and hydration products of CPB were analyzed by scanning electron microscope (SEM), X-ray diffraction (XRD), fourier transform infrared spectroscopy (FTIR), and mercury intrusion porosimetry (MIP). Finally, the hydration of the slag-based cementitious material binding tailings was explored. The results of this study can not only help reduce the backfilling cost and promote the large-scale application of CPB but also provide a reference for the reuse of solid wastes (e.g., tailings and slag) to mitigate environmental contamination.

2. Materials and methods

2.1. Tailing samples

The tailing specimens used in this study were obtained from a molybdenum mining site in Luanchuan County, Henan Province, China. After being transported to the laboratory, the tailings were mixed using a mixer before sample preparation to homogenize the material. The chemical compositions and basic properties of the tailing samples are given in Table 1. SiO_2 is the major mineral component at 38.71% by weight. The other main components are CaO (13.98%), MgO (8.75%), Al_2O_3 (8.08%), and Al_2O_3 (8.06%). In addition, the gradation of the tailing plays a vital role in the performance of CPB. A well-graded material contains an equal representation of all particle sizes with an ideal uniformity coefficient (C_u) of 4–6 and curvature coefficient (C_c) of 1–3 [53]. For the tailings in this study, the values of C_u and C_c were 4.5 and 1.3, respectively. These results suggest that the tailings utilized in this research are well-graded.

Table 1. Chemical and physical characteristics of the tailings used in the tests.

Chemical composition	Mass (wt.%)	Physical properties	Values
SiO_2	38.71	Specific gravity (g/cm^3)	2.76
Fe_2O_3	8.06	Bulk density (g/cm^3)	1.29
K_2O	2.06	Specific surface (cm^2/g)	5675
Na_2O	1.98	D_{10} (μm)	12.1
CaO	13.98	D_{30} (μm)	29.7
MgO	8.75	D_{50} (μm)	45.1
Al_2O_3	8.08	D_{60} (μm)	54.7
MnO	0.59	D_{90} (μm)	201.4
SO_3	2.04	C_u*	4.5
P_2O_5	0.54	C_c**	1.3

Notes: C_u: coefficient of uniformity, $C_u = D_{60}/D_{10}$. C_c: coefficient of curvature, $C_c = (D_{30})^2/(D_{60} \times D_{10})$.

To identify the complicated mineralogical composition of the molybdenum tailings, the sample was characterized using XRD. The mineralogical composition of the homogenized molybdenum tailing specimen is shown in Figure 1. The main components identified in the molybdenum tailings are dolomite, kaolinite, feldspar, and phlogopite phases, with minor phases of calcite, chlorite, and quartz. This agrees well with the chemical composition which indicates the high proportions of SiO_2, CaO, MgO, and Al_2O_3 (Table 1).

2.2. Slag-based cementitious material preparation

The binder cost typically has a significant influence on the operational costs of a paste backfill plant. Artificial pozzolanic products such as BFS, silica fume, and fly ash can not only improve the strength of the paste backfill but also decrease the binder wastage and operating costs of CPB [22, 24, 28, 40, 54]. This research explores the preparation of slag-based cementitious material using BFS as the main material and gypsum, clinker, and activator as the additives in the non-calcined condition. The BFS was provided by a steel plant, in Henan Province, China. Gypsum was purchased from the Yongtai Gypsum Group Co. Ltd., Sanmenxia, China. Clinker was obtained from the Mengdian Cement Co. Ltd., Xinxiang, China. The OPC (P.O. 42.5) used to compare the influence of slag-based cementitious material on the CPB's compressive strength and toxicity leachability was purchased from Mendian Cement Co. Ltd., Xinxiang, China. The elemental composition of the original materials was determined by X-ray fluorescence (XRF) spectroscopy and the results are given in Table 2. However, BFS is usually a low-crystalline phase compound, and its high activity may be attributed to the higher content of the glass phase. The XRD spectra of the BFS is shown in Figure 2, which is consistent with its chemical composition. Mineralogical analysis showed that the slag consisted largely of a vitreous phase and a minor melilite phase.

The slag-based cementitious materials proposed in the study is composed of 69 wt.% BFS, 23 wt.% gypsum, 5 wt.% clinker, and 3 wt.% activator, which are blended and ground for approximately 20 min to act as the binder. According to the method stipulated in the test methods for cement mortar (GB/T 1345-2005 [55], GB/T 1346-2011 [56], GB/T 8074-2008 [57], GB/T 17671-1999 [58]), the basic properties of the slag-based cementitious material were measured and the results are given in Table 3.

2.3. CPB preparation

The CPB specimens were manufactured by homogenizing the tailings and binder (slag-based cementitious material or OPC) in a mixer equipped with a double spiral. Tap water was slowly added to the dry mixture and blended using a high-speed blender for 3–5 min, eventually reaching a solid percentage of 80%. Subsequently, the fresh compound was transferred immediately into a triple mold with a side length of 70.7 mm to prepare the hardened CPB. The molds were then sealed and taken out after one day at room temperature. All the hard samples were allowed to cure in a humidity chamber maintained at a temperature of 20 ± 2 °C and approximately 90% relative humidity for the curing period. After the curing, the hardened samples were tested by UCS, TCLP, BCR, SEM, XRD, FTIR, and MIP to determine their compressive strength, toxicity leachability, and microstructure. In total, the slag-based cementitious material

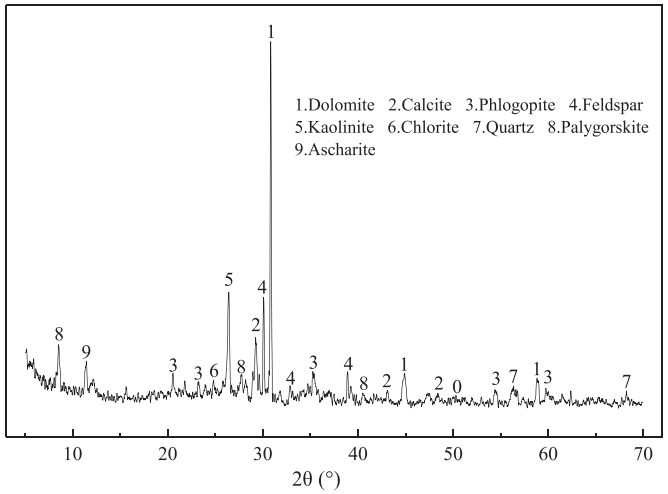

Figure 1. XRD pattern of tailings sample.

Table 2. Chemical composition of raw materials used in the experiments (wt.%).

Compounds	BFS	Clinker	Gypsum	OPC*
CaO	29.14	59.83	32.41	60.51
SiO_2	41.23	21.48	1.21	20.95
Fe_2O_3	1.89	3.63	0.39	1.97
Al_2O_3	13.54	4.72	0.61	5.13
MgO	6.85	3.70	1.05	1.68
K_2O	1.09	0.54	0.08	0.85
Na_2O	0.81	0.69	0.16	0.43
SO_3	0.56	0.95	45.25	2.72

Notes: OPC = Ordinary Portland Cement (P.O. 42.5).

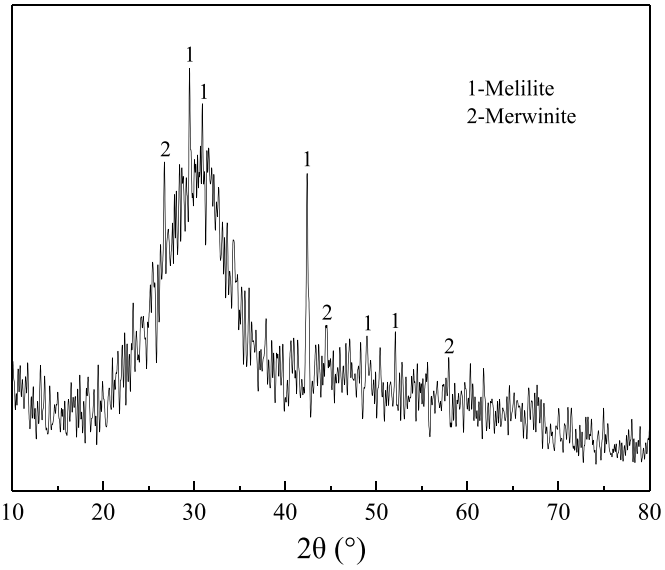

Figure 2. XRD pattern of BFS.

Table 3. Basic properties of slag-based cementitious material and OPC used in the experiments.

Physical properties		Slag-based cementitious material	OPC
Specific density (g/cm^3)		2.83	3.18
Specific surface area (cm^2/g)		3690	3980
Water requirement of normal consistency (%)		30.8	25.9
Residue on 80 μm sieve (%)		2.1	3.2
Initial setting time (min)		70	135
Final setting time (min)		140	275
UCS (MPa)	3 days	15.3	16.7
	7 days	20.5	31.9
	28 days	29.3	43.1

additions were 5%, 10%, 15%, and 20% based on the weight of the CPB, and these samples were denoted as S5, S10, S15, and S20, respectively. For comparison, the proportion of added binder was 20% by weight when using OPC as a group and named C20. The mix proportions of the CPB samples are given in Table 4.

2.4. Characterization of CPB

2.4.1. Uniaxial compressive strength tests

To quantify the mechanical properties of the CPB specimens, UCS tests were performed on the cured samples for different binder types and dosages. Compressive strength of CPB sample was calculated based on the method suggested by the ASTM C109/C109M-2016 standard [59]. The UCS was tested by a digital pressure loading machine (JYE-300, Cangzhou Yaxing Test Instruments Corporation, China) with a capacity of 300 kN, and the speed was 1 mm/min. Each specimen was in triplicate to ensure repeatability and accuracy and the mean value of results was used for analysis.

2.4.2. Leaching toxicity tests

The leaching toxicity test of the HMs was conducted as per the TCLP defined by the United States Environmental Protection Agency (USEPA). The TCLP is among the most popular ecological assessment techniques globally and is very helpful in detecting the dissolution and migration of HMs in solid waste [13]. Therefore, this study employs TCLP to discover the toxicity leaching properties of CPB. The CPB specimens were crushed to particle size less than 9.5 mm for the TCLP. The leaching agent was prepared by acetic acid and deionized water with a pH of 2.88 ± 0.05. The leaching agent and the crushed particles were mixed at a liquid-to-solid ratio of 20:1 (L/Kg) and vibrated for 18 h at 30 rpm under ambient conditions. Each leachate was vacuum filtered through a 0.45 μm membrane filter and leaching concentration of HMs was analyzed with inductively coupled plasma optical emission spectroscopy (ICP-OES).

2.4.3. Sequential chemical extraction

In addition to the leaching characteristics, the chemical speciation of HMs in mine tailings plays an important role in the possible environmental effects. In this study, the HMs distribution was investigated by modified BCR sequential extraction procedures. This results in four HMs fractions, namely, extraction of exchangeable fraction, reducible fraction, oxidizable fraction, and residual fraction, which were classified according to the methods mentioned in Table 5. HMs in each fraction were determined by ICP-OES.

2.4.4. Microstructure analysis

SEM, XRD, FTIR, and MIP examinations were performed on selected CPB specimens to observe and identify the crystalline substances, morphology, porosity, and structure of the hydration products. The fractured CPB specimens were placed in absolute ethyl alcohol to finish the reaction process. After 24 h the debris was filtered to remove the alcohol and dried in an oven until the weight became constant. Fragments of CPB were coated with a conductive metal, and the CPB microstructure was analyzed by a JSM-5610LV SEM instrument. The samples were ground using a 45-μm sieve and XRD analysis was carried out to reveal the mineralogical characteristics. FTIR spectroscopy of samples was accomplished with Thermo Scientific Nicolet IS 20. MIP test was conducted on dried CPB by using an Autopore IV 9520 pressure mercury porosimeter.

Table 4. Raw material proportions of the CPB specimens.

Material	S5	S10	S15	S20	C20
Slag-based cementitious material (%)	5	10	15	20	0
Tailings (%)	95	90	85	80	80
OPC (%)	0	0	0	0	20

Table 5. BCR chemical speciation analysis of HMs.

Step	Fraction	Reagents/1 g of sample	Conditions
F1	Exchangeable	40 ml 0.11 M acetic acid (CH_3COOH)	Shaking 16 h at 22 ± 5 °C
F2	Reducible	40 ml 0.5 M hydroxyl ammonium chloride ($NH_2OH{\cdot}HCl$)	Shaking 16 h at 22 ± 5 °C
F3	Oxidizable	10 ml 8.8 M hydrogen peroxide (H_2O_2) 50 ml 1.0 M ammonium acetate (CH_3COONH_4)	Shaking 1 h at 22 ± 5 °C and digested for 1 h at 85 ± 2 °C Shaking 16 h at 22 ± 5 °C
F4	Residual	Aqua-regia (7 ml 35% HCl + 2.3 ml 70% HNO_3)	Occasional agitation

3. Results and discussion

3.1. HMs characterization in tailing samples

The pH values of the tailings ranged from 4.6 to 6.5 with an average value of 5.7, indicating a slightly acidic environment. The acidity of tailings enhances the fluidity of the potentially toxic HMs and increases the possibility of environmental damage. The total HMs content and TCLP results for the tailing samples were analyzed as shown in Figure 3.

As shown in Figure 3, the results indicated that the Pb, Cr, Cu, and Cd contents in the tailings were significantly higher than the corresponding background values associated with the soil in Henan Province [60]. Particularly, Pb was the element with the highest concentration of 1377 mg kg^{-1}, which was approximately 61.75 times the allowable value. If the Chinese agricultural soil environmental quality control criteria (GB 15618-2018) [61] are regarded as the baseline, the Pb, Cr, Cu, and Cd contents exceed the maximum allowable values, indicating a risk of contamination. It is particularly noteworthy that the Pb and Cd contents are not only higher than the risk screening values but also exceed the risk intervention values. In addition, the leachability of the HMs in the tailings was determined using the standard TCLP procedure. The results indicated that the leachate concentration of Cr, Cu, and Cd in the leachate was below the limit prescribed by GB 5085.3-2007 [62]. In particular, the leachate concentration of Pb was 12.65 mg L^{-1}, which exceeded the acceptable limit value by 2.5 times. This indicates the need for appropriate preventive measures for environmental pollution.

To evaluate the environmental impact of HMs present in the tailings, it is necessary to analyze the mobility and possibility of the release of HMs along with their availability in the tailings depending on their chemical forms. The BCR sequential chemical extraction results of HMs in the tailing samples are shown in Figure 4. As shown in Figure 4, the percentage distribution of Pd and Cb in different chemical forms differed from that of Cr and Cu. The partitioning fraction of Cd and Pb was nearly similar. Cd (59.15%) and Pb (35.41%) had the highest concentrations in the exchangeable fraction, thereby indicating that Cd and Pb presented considerable ecological hazards. The reducible fraction contained the main form of Cu present in the tailing samples (58.14%), and the percentages of Cu in the exchangeable, oxidizable, and residual fractions were lower (15.81%, 14.51%, and 11.54%). Previous studies [3, 63, 64, 65] showed that HMs with a large proportion of the reducible fraction were sensitive to changes in the pH or redox conditions of the medium, and were easily released into the environment under acidic conditions. The potential environmental risks posed by the reducible fraction of Cu should not be ignored. Unlike Cu, the distribution of Cr differed considerably among the examined samples. Cr was mainly detected in the residue fraction (45.36%), while only 12.65%, 20.67%, and 21.32% of the Cr were found in the exchangeable, reducible, and oxidizable

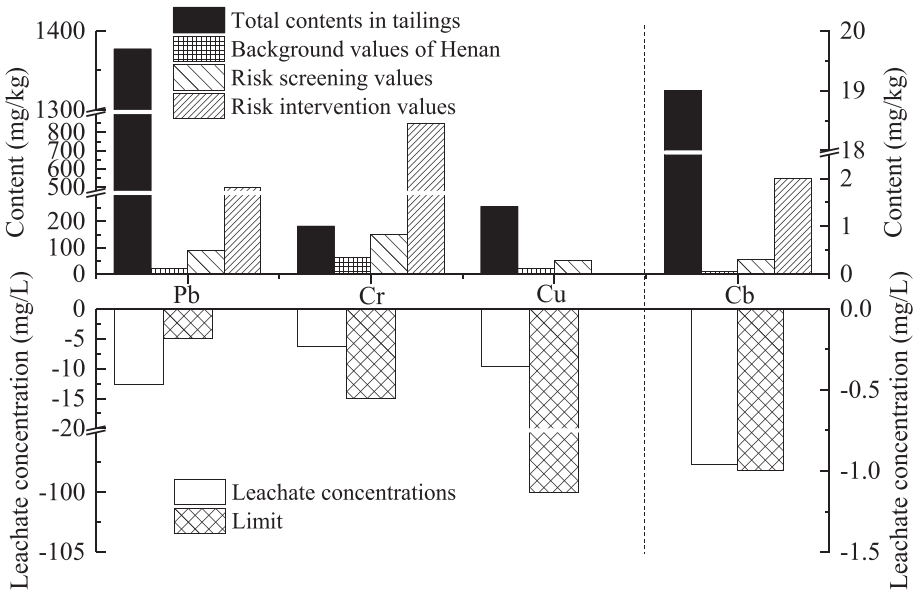

Figure 3. Total HMs content and TCLP results in tailing samples.

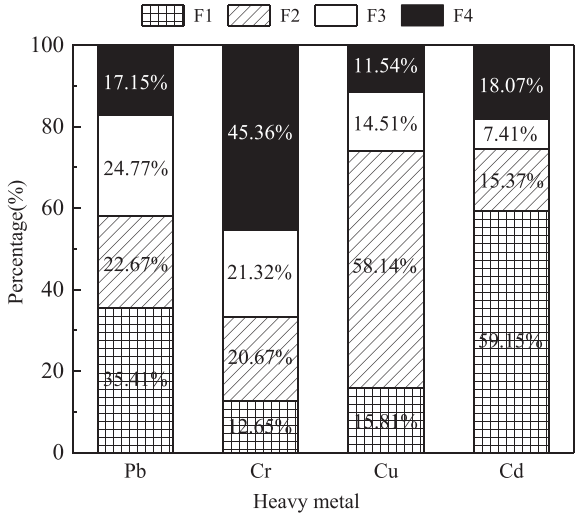

Figure 4. Chemical fractions of HMs in tailing samples. F1: exchangeable fraction; F2: reducible fraction; F3: oxidizable fraction; F4: residual fraction.

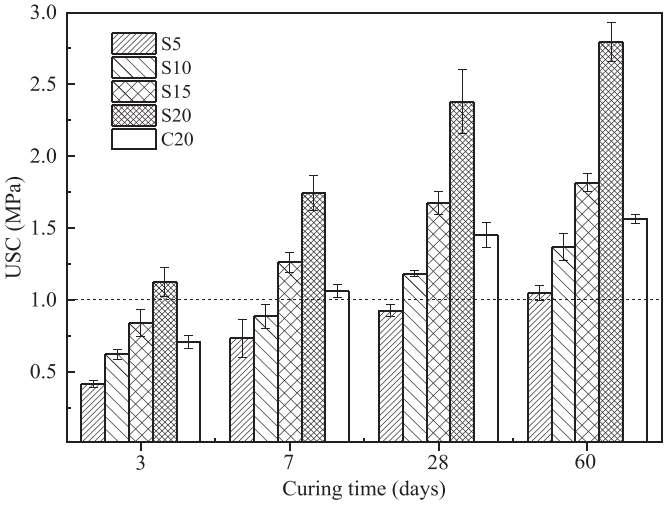

Figure 5. UCS test results of CPB specimens.

fractions, respectively. The results indicated that Cr showed the strongest retention characteristics.

3.2. Mechanical properties of CPB

The quantity of binder and the curing time have a remarkable impact on the stability of CPB, and strength is the most critical factor to access the mechanical stability of CPB. The UCS tests results of the CPB specimens were presented in Figure 5. The dashed line represents the mechanical strength requirement of mine fillings. It shows the variation of UCS in CPB with different slag-based cementitious material dosages (5%, 10%, 15%, and 20%) and curing times (3, 7, 28, and 60 days). The comparative experiment was carried out with a 20% OPC content.

At present, there are no universal standards for the compressive strength requirements of CPB used during exploration and mining. However, some earlier studies [66, 67, 68, 69] had determined the required strength value for the excavation and mining stability of the backfill as up to 1.0 MPa at 28 days. As shown in Figure 5, the UCS of the CPB specimens meets the requirement for mine filling after a curing time of 28 days. These results revealed that the strength of the CPB samples showed a considerable increase with increasing binder dosage at all curing times. Sample S5 had the lowest compressive strength, reaching approximately 0.42 MPa, 0.73 MPa, 0.92 MPa, and 1.05MPa after curing for 3, 7, 28, and 60 days, respectively. The highest strength was noticed for sample S20, reaching approximately 1.13 MPa, 1.74 MPa, 2.38 MPa, and 2.80 MPa after curing for 3, 7, 28, and 60 days, respectively. When the dosage of slag-based cementitious material increased from 5% to 20%, the UCS values of the samples increased by 169%, 138%, 159%, and 167% after 3, 7, 28, and 60 days, respectively. This indicated that the increase in slag-based cementitious material dosage considerably improved the mechanical strength of CPB as the higher hydration rate and increase of hydration products in the slag-based cementitious material leads to the development of the compressive strength of CPB. The results indicated that the quantity of slag-based cementitious material had a positive impact on the increase in strength regardless of the hydration time.

From Figure 5, it could be seen that the compressive strength of CPB increased gradually with the curing time, which revealed that there was a significant positive correlation between the two factors. As the curing

time increased from 3 days to 60 days, the UCS values increased by 153%, 120%, 116%, and 148% for the tailings solidified by 5%, 10%, 15%, and 20% of the slag-based cementitious material, respectively. These results revealed that the mechanical strength of all the paste backfill samples increased visibly with the curing period owing to the continuous pozzolanic reaction and the generation of many hydration products such as calcium silicate hydrate (C–S–H), ettringite, and portlandite [34, 36, 53, 70, 71].

Regardless of the binder dosage and curing time, the slag-based cementitious material produces a stronger backfill material for the molybdenum tailings. However, in contrast to slag-based cementitious material, when 20% OPC was used and the specimens were cured for 3, 7, 28, and 60 days, the magnitude of UCS was much lower at approximately 0.72 MPa, 1.06 MPa, 1.43 MPa, and 1.55 MPa, respectively. These values were comparable to the content of 10%, which means that only half the quantity of slag-based cementitious material is required compared to the cement for the same strength of CPB. To a certain extent, the mechanism of strength development is different. For example, the strength of CPB rises rapidly when slag-based cementitious material is used, while a non-clear increase is observed on CPB samples that use OPC.

3.3. Toxicity leachability of CPB

TCLP tests were conducted to reveal the leaching behavior of HMs in CPB samples. The HMs leaching results of CPB with different binder dosages after curing for 3, 7, 28, and 60 days are shown in Figure 6. The dashed line represents the leachate concentration of Pb, Cr, Cu, and Cd from the original tailing sample.

As shown in Figure 6, the leachate concentrations of HMs from the CPB decreased with the increase in slag-based cementitious material in all the samples, and the HMs in the leachate from CPB stabilized by slag-based cementitious material were very low and within the prescribed limits. In addition, regardless of whether the tailings were solidified by slag-based cementitious material or OPC, the increased curing time reduced the concentration of HMs that leached from the CPB. These results revealed that the solidification of the tailings could effectively reduce the leaching concentration of HMs, and maintained it within the national standard requirement (GB 5085.3-2007) [62]. Therefore, the slag-based cementitious material showed good immobilization capability for the HMs material. The TCLP test results showed that the leachate concentration of Pb in the original tailings was approximately 12.65 mg L^{-1}, which was much higher than the prescribed limits (5 mg L^{-1} in China). After CPB treatment, the leachate concentrations of Pb in all the CPB samples declined evidently in the range of 0.19 and 2.64 mg mL^{-1}, which were far below the prescribed limits, with a decrease ranging from 79.13% to 98.50%. Sample S20 after 60 days of curing presented better HMs consolidation capacity owing to the various hydrates that facilitate the chemical fixation and physical encapsulation effects [72]. It indicates that CPB benefits exceedingly concerning the leaching toxicity of tailings and eventually reaches a relatively stable state of leaching during long-term storage. Especially, slag-based cementitious material can inhibit the leaching of HMs in the CPB and reduce the toxicity of tailings in contrast with the untreated original tailings. This phenomenon is mainly due to the time- or dosage-dependent hydration reaction of silicates present in the BFS, the pozzolanic reaction between the $Ca(OH)_2$ from the clinker, hydrated BFS, and active components in the tailings, precipitation reaction of HMs, and absorption of C–S–H formed in the CPB [63]. A higher binder dosage or longer curing time makes the above reactions more vigorous and consequently decreases the leaching concentrations of HMs in the CPB. Based on the above, the leachable HMs

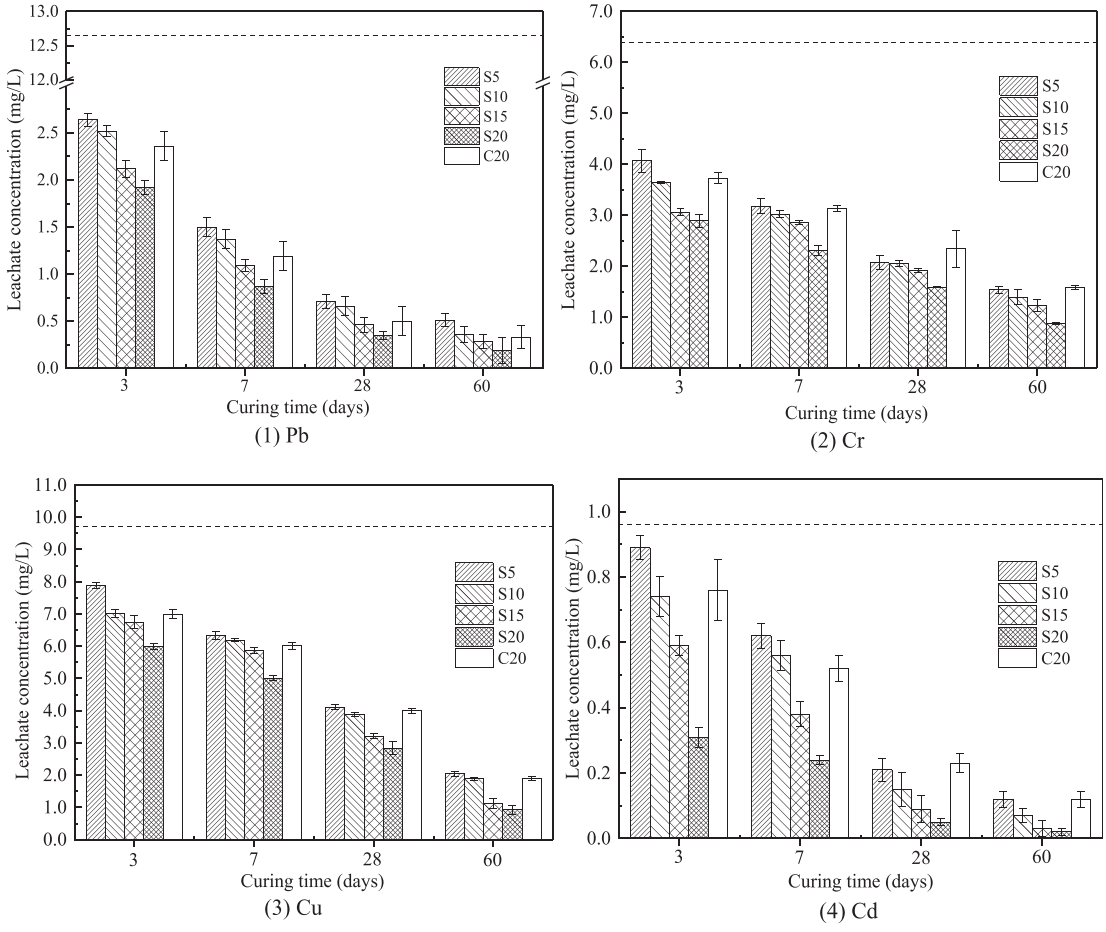

Figure 6. HMs leaching results of CPB specimens.

from CPB decreased significantly with slag-based cementitious material, indicating that the leaching risk of HMs in the tailings can be mitigated effectively by using slag-based cementitious material. It was revealed that slag-based cementitious material could not only have a promotion effect on the UCS of CPB but also reduce the leaching concentration of HMs in the tailings. The results of toxicity leaching are coincident with the results of the above-mentioned compressive strength wherein the higher binder dosage decreased the leachability of HMs by generating more hydration products. Earlier studies [39, 73, 74] show that the difference in the leaching behavior of HMs is not only related to their initial content in tailings but is also affected by the chemical speciation of the HMs. This finding is proved based on the HM distribution presented in Section 3.4.

In addition, the leached HMs concentrations in the OPC-treated tailings were higher than that of the slag-based cementitious material treatments under the same additives. In contrast with slag-based cementitious material, the leaching concentrations of HMs in sample C20 were like those in sample S10. The result reveals that the slag-based cementitious material dosage is lower than half the OPC dosage, which achieves the same solidification effect.

3.4. Sequential leaching results of CPB

The migration and toxicity of the HMs are strongly dependent on their specific chemical speciation distributions. The results of the BCR sequential extraction of the HMs in the CPB samples for different curing times and binder dosages are shown in Figure 7. The F1 fraction of the HMs leach easily in nature, resulting in high toxicity; the F2 and F3 fractions are available in the reducing and oxidizing surroundings, which indicate potential toxicity. Meanwhile, the F4 fraction is unavailable for leaching and represents the nontoxic fraction [73, 75].

The different fractions have varying effects on the chemical stability of HMs in the CPB. As shown in Figure 7, the chemical speciation of HMs was observed to transform when the tailings were treated with slag-based cementitious material. Compared with the chemical speciation of the HMs in the raw tailing samples, the HMs changed into more stable forms in all the CPB samples. However, the proportion of each form changed differently. For Pb, the major transformation of speciation occurred from the F1 fraction into the F4 fraction, which causes an increase in the F4 fraction from 17.15% to 91.74%. For Cd, the contents of the F1 and F4 fractions both decreased, while the F2 and F3 fractions increased constantly. Most of the F2 fraction of Cu and Cr were transferred into the F3 fraction, leading to a considerable increase of the F3 fraction from 14.51% to 78.02% and from 21.32% to 43.40%, respectively. It can be concluded that the HMs in the CPB transform to a stable form after curing. This transition can be used to explain the reduction of HMs mobility in the CPB. As shown in Figure 7, the contents of the F4 fraction increased during the period from 3 to 60 days, which revealed that slag-based cementitious material displayed a good stabilization/solidification capacity for HMs.

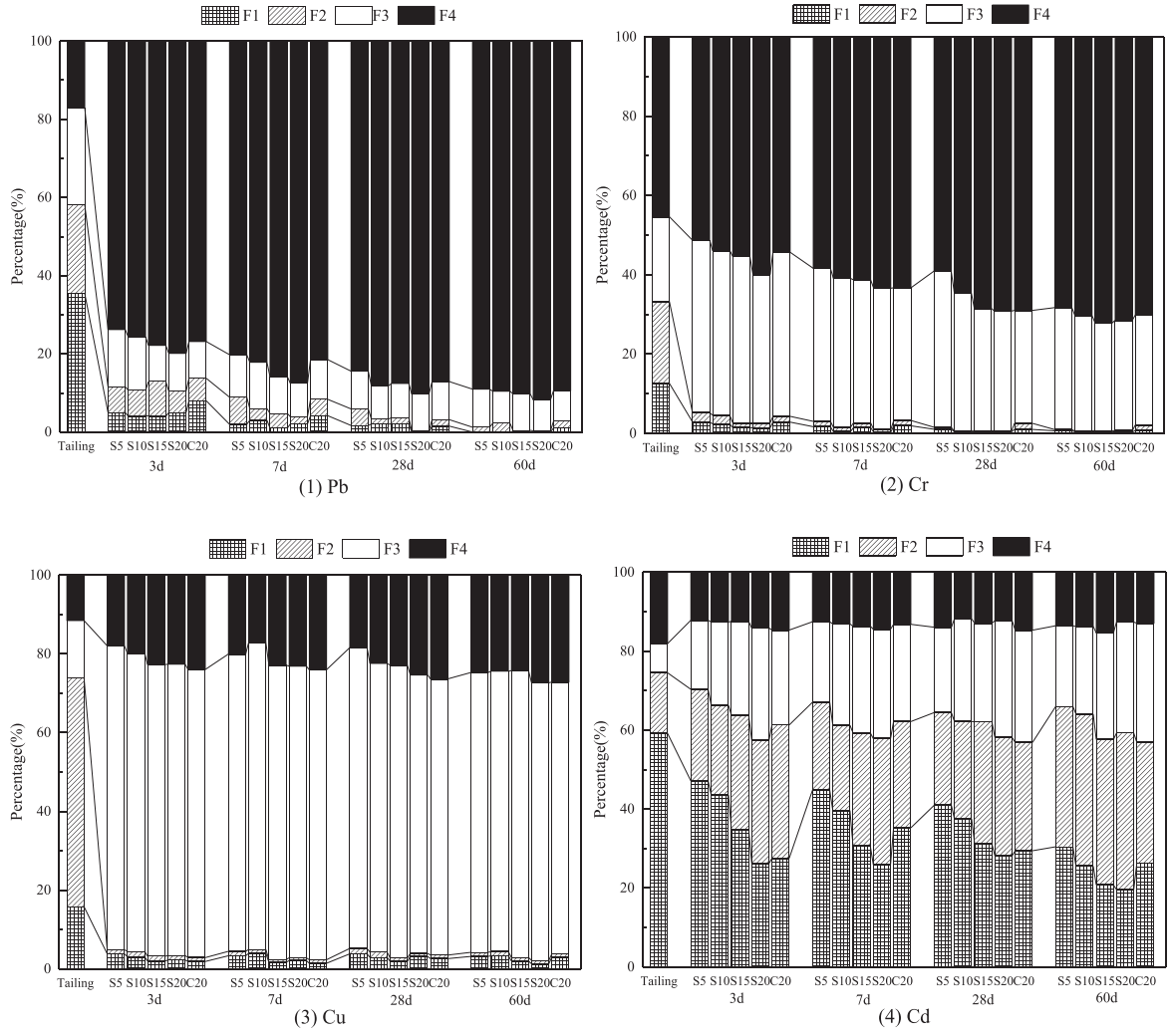

Figure 7. Chemical speciation of HMs in CPB specimens. F1: exchangeable fraction; F2: reducible fraction; F3: oxidizable fraction; F4: residual fraction.

3.5. Microstructure characteristic of CPB

The CPB is an inhomogeneous polyphase system composed of a solid phase that has abundant reaction products, air, and water in the pore spaces [76, 77, 78]. Therefore, it can be considered to be similar to a heterogeneous polypore paste-filled body [79, 80]. To survey the internal microstructure visually, SEM tests of the sample S20 were performed in Figure 8, which illustrated the SEM of sample S20 after curing for 3, 7, 28, and 60 days, respectively.

Rod-like ettringite and flocculent gel overlap in the CPB samples with different curing times. A small quantity of the amorphous phase may be observed in Figure 8(1). Considerable porosity still exists in the CPB after curing for 3 days, and the pores are very open and partially connected. The water and binder collected in the pores inhibited the complete reaction of the tailings and the slag-based cementitious material. The particles are not bonded closely, and the entire sample is comparatively loose. In contrast to Figure 8(1), the microstructure of Figure 8(2) is denser, and the number of hydration products increases greatly, among which a few needle-shaped particles may be observed. Although hydration products such as C–S–H and ettringite are present, they are not yet connected extensively to overlap all the tailing particles. Significantly, the porosity between the grains decreased greatly, and the surfaces of the CPB samples had a comparatively flat morphology and dense microstructure after curing for 28 days. Figure 8(4) shows that abundant C–S–H gels and needle-like ettringite are filled into the pores, the hydration products bind the grains together resulting in a more compact structure, and no obvious gaps could be observed in sample S20 after curing for 60 days. It also shows that sample S20 developed a dense, glassy microstructure as the curing time increased. This can be attributed to the continuous hydration reaction in the CPB samples, spherical particle clusters of the C–S–H gels, needle-like crystals of ettringite, and other hydration products that form in the vicinity of the tailing grains [79]. The quantity of the hydration products in the reaction plays an important role in the physical properties of CPB. The pictures showed that the size of the rod-like crystal body was approximately 3–5 μm. The distribution of these ettringite crystals inside the CPB was exceptionally inhomogeneous, causing the crystals to grow in random directions. Thus, a majority of the original pores in the backfill body are filled with hydration products, which makes the structure denser and increases strength. The results demonstrate an improvement in the CPB microstructure after different curing periods, which agrees with the compressive strength development with curing periods shown in Figure 5. However, the major hydration product of OPC is calcium hydroxide, which is porous and hence, very unfavorable to the development of strength [81]. Thus, the effect of CPB using slag-based cementitious material is better than that when OPC is used.

XRD is a rapid analytical technique mainly used to identify the characteristics of crystalline substances [82, 83]. The mineral phase characterization of the hardened backfill sample S20 cured for 3, 7, 28, and 60 days was conducted by the XRD test as shown in Figure 9.

From the XRD analysis of sample S20, it can be found that the number of hydration products exceeded that of other groups owing to the

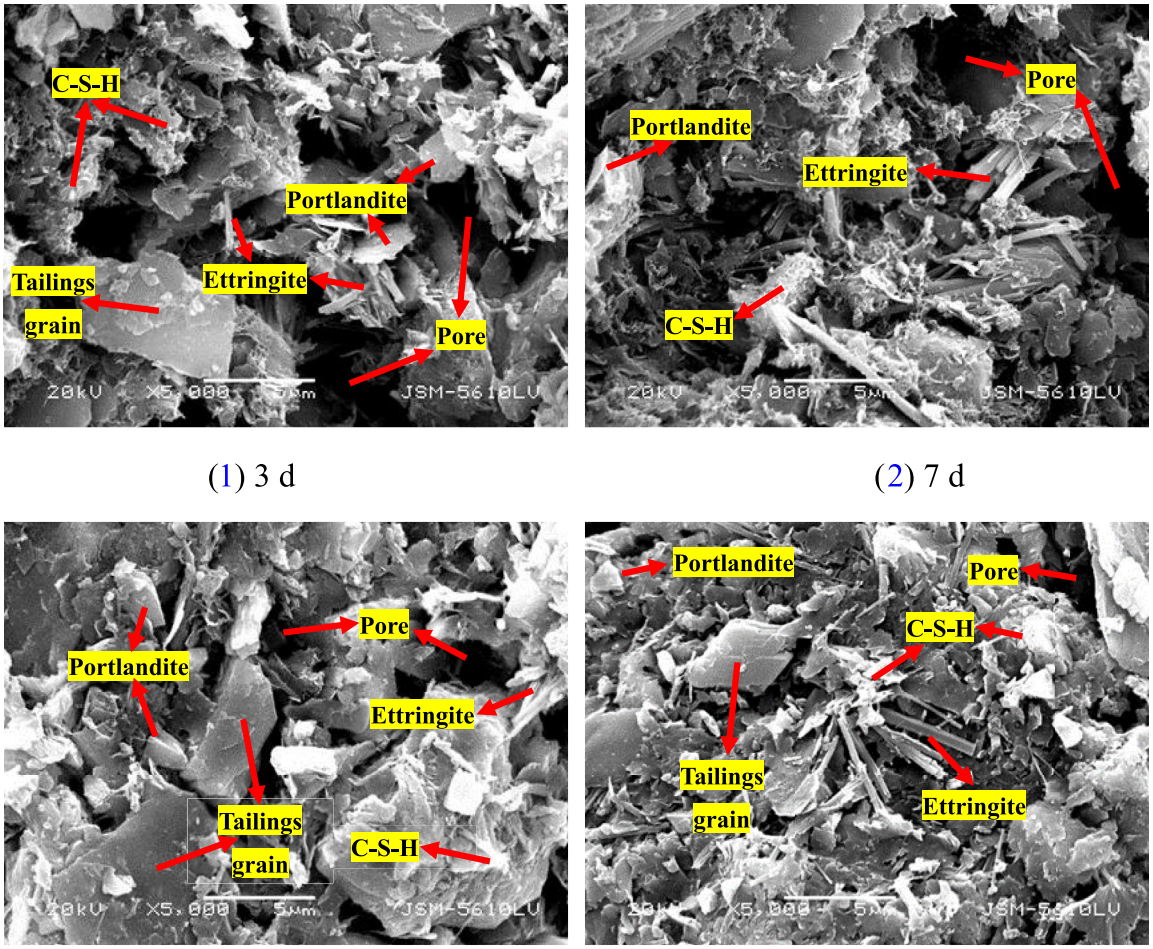

Figure 8. SEM images of sample S20 after different curing times.

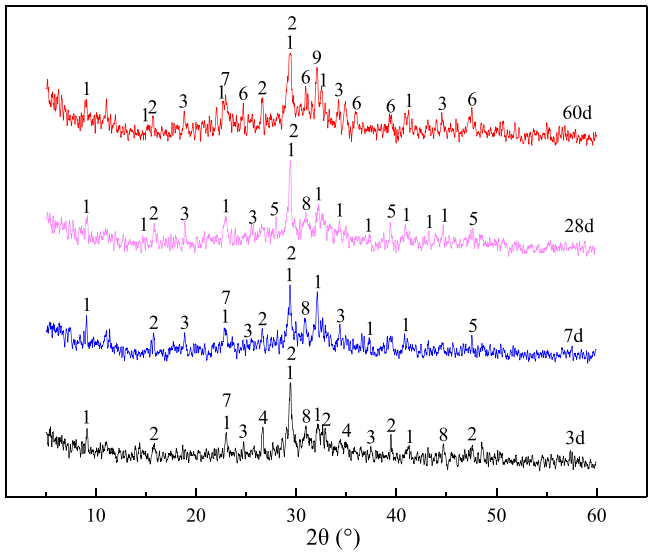

Figure 9. XRD patterns of sample S20 at different curing times. 1—Ettringite 2—C-S-H 3—Portlandite 4—C_3S 5—Thaumasite 6—Scawtite 7—Calcite 8—Dolomite 9—C-A-H.

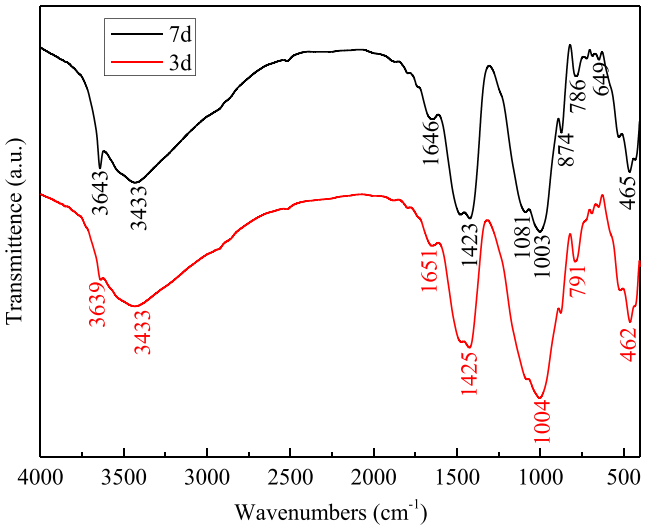

Figure 10. FTIR patterns of sample S20 at 3 and 7 days.

increased curing time. The abundant hydration products support the visual SEM observations (Figure 8). The primary hydration products of sample S20 are ettringite, C–S–H, hydrated calcium aluminate (C-A-H), portlandite, thaumasite, and scawtite. When the curing time is extended, the peak proportions of the ettringite and C–S–H phases increase in the CPB specimens, which agree with earlier studies on alkali-activated slag-based materials [84, 85]. In addition, it was found that a small quantity of tricalcium silicate (C_3S) was formed when the curing period was 3 days, but this was not observed for other curing durations. It is particularly noteworthy that the peak of ettringite in sample S20 is quite prominent in the CPB. Compared with the XRD pattern of the raw tailings, the peak values of dolomite and calcite decreased significantly, indicating that these mineral materials might be participants in the reaction. In addition, the diffraction peaks that characterize thaumasite and scawtite were also obvious after curing for 28 days and 60 days, respectively. The emergence of carbonate confirmed that carbonation occurred during the CPB processing.

To further investigate the solidification mechanism of CPB by using slag-based cementitious material, the functional groups on the surfaces of sample S20 were characterized by FTIR. The FTIR patterns of sample S20 after being cured for 3 and 7 days are shown in Figure 10.

As can be seen, the FTIR curves of CPB after different curing times were basically the same. After curing for 3 days, asymmetric stretching vibrations of O–H bonds in crystalline water at 3433 cm^{-1} and bending vibrations of H_2O molecules at 1651 cm^{-1} could be seen in sample S20, indicating that the slag-based cementitious material hydration reaction produced a large amount of product containing crystalline water or gel, which was characteristic of the vibrational absorption of crystalline water [42, 77]. After curing for 7 days, the strong absorption peak at 3643 cm^{-1} corresponded to the stretching vibration of the hydroxyl group on the surface of the octahedron. The absorption band at the position of 1081 cm^{-1} belonged to the asymmetric stretching vibration of SO_4^{2-} [77]. The adsorption peak of 649 cm^{-1} was caused by bending vibration of SO_4^{2-}. It was evident that these absorption peaks could be characterized as vibration peaks of ettringite, which was consistent with the results of XRD and SEM analysis. The characteristic peaks located between 780 cm^{-1} and 1005 cm^{-1} were caused by the asymmetric stretching vibration of the Si–O(Al) in C–S–H gels [44]. The peak attributed to the tetrahedral-tetrahedral ion vibration of silicates had been shifted from 791 to 786 cm^{-1} after different curing times, indicating the breaking down of chemical bonds during activation and forming new amorphous products [86]. The FTIR spectra showed a broad peak between 1100 and 1000 cm^{-1} assigned to the asymmetric stretching vibration of Si–O–Al or Al–O–Si, which were characteristic absorption bands indicative of successful hydration reaction [86]. All the end products showed bending vibrations of Si–O–Si and O–Si–O at 465–460 cm^{-1} [87]. In addition, the peaks at 1423 cm^{-1} and 1425 cm^{-1} characterized the symmetrical vibration of the O–C–O in CO_3^{2-}, which was caused by the carbonization of the sample in air [77].

As shown in Figure 11, deconvolution in the region from 1200-800 cm^{-1} using Gaussian fitting [88] further revealed the formation of slag-based cementitious material reaction products. The absorption peaks observed at 1105 and 1115 cm^{-1} could be associated with the asymmetric stretching vibrations of Si–O bands in the sample [87]. Meanwhile, the peaks detected at 989 and 995 cm^{-1} in sample could be attributed to the stretching vibrations of silicates bonded with the activator, such as Si–O, Ca–O and other structures [86]. In addition, the bands near 874 and 857 cm^{-1} were weak and mainly related to Si–OH bending or tetrahedral bending vibrations [86]. On the whole, the reaction process made the characteristic peak of Si–O shift significantly, indicating that some minerals were affected by hydration reaction.

MIP test is often used to gain further insight into the porosity development of CPB. The cumulative porosity and pore size distribution of S20 specimen were inspected through MIP for 3 and 7 days curing, as illustrated in Figure 12. The effects of curing time on the pore structure characteristics of S20 specimen were listed in Table 6.

The results of the MIP test clearly showed that the curing period had influenced the microstructure of CPB. It can be seen that S20 specimen at 7 days had a lower cumulative porosity and a finer pore structure than at 3 days as shown in Figure 12, which indicated the cumulative porosity of sample decreasing with the extension of curing time. Related researches showed that the hydration products strongly modified the pore structure (i.e., reduce the porosity) of the CPB [34, 40, 71]. The slag-based cementitious material could produce ettringite crystal intermixed with C–S–H gels on a nanometer length scale. The cumulative porosity curves and pore size distribution curves demonstrated that the accumulation of many hydration products in the pores with the extension of curing period could effectively optimize microstructures and reduce the pore size [52]. Table 6 confirmed that the curing time had influenced the porosity and pore structure characteristics of CPB. Specifically, the porosity was decreased from 35.72% at 3 days to 25.47% at 7 days. Higher amount hydration products could fill the pores among particles, leading to lower porosity [23]. Both the average pore diameter and median pore diameter tended to become finer with increasing curing times. The average pore diameter at 3 and 7 days were 86.88 nm and 40.32 nm, respectively. The

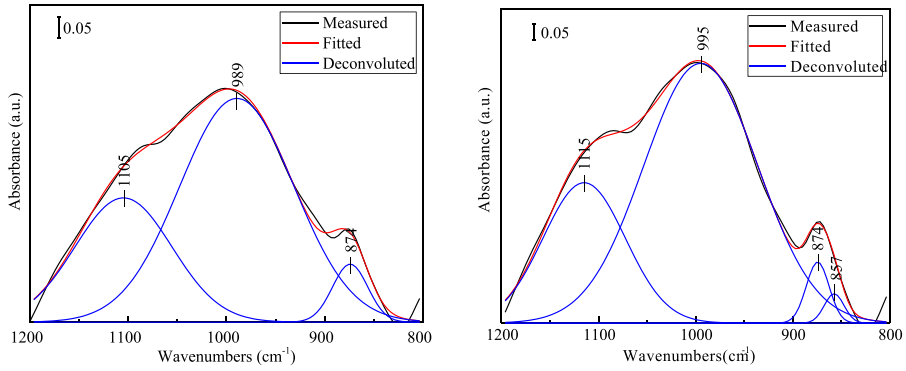

(1) 3d (2) 7d

Figure 11. Deconvoluted spectra in the 1200-800 cm^{-1} for S20 specimen.

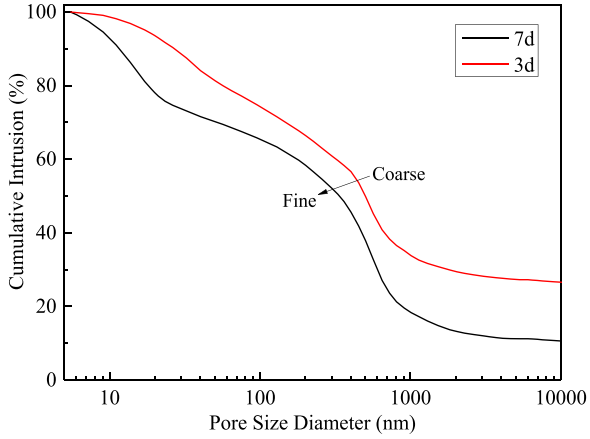

(1) Cumulative porosity

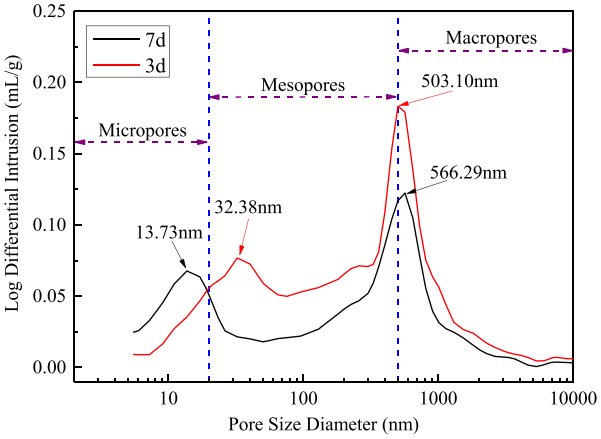

(2) Pore size distribution

Figure 12. MIP test results of S20 specimen at 3 and 7 days.

data proved that curing period promoted slag-based cementitious material hydration reaction with the formation of more compact microstructure and lower total porosity, contributing to a higher mechanical strength and a better HMs immobilization effect, as shown in Figures 5 and 6. This is consistent with the SEM results.

Table 6. Pore structure characteristics of S20 specimen from MIP data.

Curing times (days)	3	7
Porosity (%, v/v)	35.72	25.47
Total pore area (m^2/g)	10.23	12.70
Total intrusion volume (mL/g)	0.22	0.13
Average pore diameter (nm)	86.88	40.32
Volume based median pore diameter (nm)	503.33	337.13
Surface area based median pore diameter (nm)	21.98	11.88

4. Discussion

4.1. Hydration reaction of CPB

The sample S20 was subjected to SEM after 3, 7, 28, and 60 days of curing to verify the mechanical strength measurements. Early on, owing to the high porosity of CPB, the hydration products could not fill the pores, resulting in low strength. After curing for 28 days or more, a large quantity of C–S–H and ettringite appeared in Figure 8(3) and (4). The rod-like ettringite crystals were scattered around the C–S–H gel and the transition regions between the tailings and cementitious materials were narrow, which enhanced the internal connections of the CPB. The pores were compacted with hydration products, which interpenetrated each other to augment the mechanical strength of the CPB.

This phenomenon may be principally attributed to the curing time-dependent hydration reaction of the silicates in the slag-based cementitious material and the simultaneous pozzolanic reaction in the CPB. As shown in Table 2, the chemical compositions of the OPC and clinker are essentially the same, mainly involving C_3S, dicalcium silicate (C_2S), and tricalcium aluminate (C_3A). Large amounts of C–S–H, portlandite (CH), and C–A–H are derived from the hydration of C_3S, C_2S, and C_3A according to formulas (1), (2), and (3), respectively.

$$C_3S + H_2O \rightarrow C\text{–}S\text{–}H + Ca(OH)_2 \quad (1)$$

$$C_2S + H_2O \rightarrow C\text{–}S\text{–}H + Ca(OH)_2 \quad (2)$$

$$C_3A + H_2O \rightarrow C\text{–}A\text{–}H \quad (3)$$

Ettringite is one of the components that improve the stability of the filler. The rod-like ettringite is produced by a further reaction involving the rapid dissolution of gypsum to generate SO_4^{2-} and Ca^{2+} as summarized in formula (4).

$$C_3A + CaSO_4{\cdot}2H_2O + H_2O \rightarrow C_3A\underline{S}_3H_{32} \quad (4)$$

The clinker in the slag-based cementitious material dissolves in water to produce OH^-, which is distributed depending on the concentration

gradient. In alkaline environments, the OH^- ion enables the activation of the bridge oxygen bond and non-bridge oxygen bond, which reacts with the amphoteric oxide Al_2O_3 and acidic oxide SiO_2 in the slag, and accelerates the hydrolysis of the glass phase. According to the SEM, XRD, and FTIR test results, the hydration reaction process of the CPB mainly includes the following steps [89]:

The first step is the dissolution. The alkaline solution causes the surface of the active materials Al_2O_3 and SiO_2 of the slag to first react with the OH^-. The Al–O–Al, Si–O–Si, and Si–O–Al break and generate $Si(OH)_3^-$ and $Al(OH)_4^-$, which slowly dissolve and fracture the compact glassy structure. The relevant chemical reactions are formulas (5) and (6) as follows:

$$SiO_2(s) + H_2O + OH^-(aq) \rightarrow Si(OH)_3^- \quad (5)$$

$$Al_2O_3(s) + 3H_2O + 2OH^-(aq) \rightarrow 2Al(OH)_4^- \quad (6)$$

The second step is the hydration stage. The reaction products $Si(OH)_3^-$ and $Al(OH)_4^-$ dissolve in the early stages and react with Ca^{2+} and OH^- to generate C–S–H, C–A–H, etc. The chemical reactions are formulas (7) and (8) as follows:

$$2xSi(OH)_3^- + xCa^{2+} + mOH^- \rightarrow xCaO{\cdot}SiO_2{\cdot}nH_2O \quad (7)$$

$$2yAl(OH)_4^- + yCa^{2+} + mOH^- \rightarrow yCaO{\cdot}Al_2O_3{\cdot}nH_2O \quad (8)$$

Meanwhile, the particulate slag delivers more amorphous Si and Al to participate in the reaction and generate more gelling substances [30]. In addition, it can be found in Figure 9 that the mineral components of the tailings contain a certain amount of active components (e.g. dolomite, calcite, etc.), which react with the cementitious materials. The hydration reactions between the slag-based cementitious material and tailings in the CPB must be further studied in the future.

4.2. Immobilization mechanism of HMs

Based on the leaching toxicity and HMs chemical fraction of CPB, it can be shown that slag-based cementitious material is a binder with a good immobilization effect on HMs. Previous studies indicate that the immobilization mechanism of HMs is mostly physical encapsulation and chemical stabilization.

The encapsulation of HMs into a low-permeability matrix is known as physical encapsulation [4]. Hence, the permeability of the hardened samples affects the physical encapsulation of HMs. The low permeability of the samples can reduce the occurrence of naked surfaces and the mobility of the HMs. On the one hand, concerning the mineral composition and microstructure, a large quantity of gelatinous hydrated product (C–S–H) and rod-shaped crystal (ettringite) emerge, and the phase formation reduces the leachability of HMs from the CPB. This may be attributed to the production of a large number of hydration products that generate a dense structure which reduces the permeability of the hardened CPB. On the other hand, the encapsulation influence of HMs relies largely on the compressive strength because samples with higher strength can retain their integrity better than those with low strength during the leaching test [90]. From Figures 5 and 6, it is easy to determine that the leached concentrations of HMs have a negative correlation with the mechanical strength of CPB. Particularly, the encapsulation of HMs and the absorptivity of C–S–H contribute to the reduced leaching concentrations [58, 91].

HMs may be stabilized using three methods, namely, resetting of particles, changing crystal phases, and replacing parent ions. The hydration products of slag-based cementitious material, such as the C–S–H and ettringite, play a vital role in solidifying the HMs. The generation of C–S–H can not only contribute to the mechanical properties and microstructure of the CPB but also supply the hydroxyl anions required to react with HMs to immobilize with the monolith [92]. C–S–H has a high ion-exchange capacity and specific surface energy, and thus, HMs can be stabilized by symbiosis and chemical substitution between the layers. The presence of gypsum in the slag-based cementitious material can promote the generation of ettringite, which has excellent mechanical properties and ion-exchange capacity [93, 94]. Ettringite can not only stabilize HMs via surface complexes or ion exchange but is also chemically substituted between the crystal columns and the passageway to consolidate the HMs [90, 94]. It indicates that ettringite can transform the chemical speciation of HMs from an unstable form to a stable one in the CPB. The immobilization of HMs in the CPB will be improved by the transformation of these HMs to a chemically stable phase [65]. It can be observed from Figure 6(1) that the residual fraction of Pb increases when the tailings are treated with slag-based cementitious material, resulting in the leached concentration of Pb decreasing continuously.

HMs can also be involved in the hydration reaction. As the hydration reaction proceeds, HMs transform slowly into calcium silicate hydration products that enter the crystal body via lattice immobilization, which exists as a more stable structure. Therefore, it can be found that the results are analogous to the consolidation process in the cement system [90]. As a result, the more hydration gel that is produced, the more conducive the situation becomes to obtain better stability. When the HMs become crystalline and the chemical combination of these HMs enter into the silicate or aluminosilicate frameworks, it indicates that the HMs can react with silicate or aluminosilicate to produce insoluble substances, the consolidation of which produce the vitreous phase [94]. In addition, the polymerization of Si will increase with the hydration reaction, generating a precursor with a zeolite-like frame existing as nesosilicate. This frame provides adequate sorption capacity and high binding potential energy with HMs [39]. To understand the relationship between the leaching concentration and morphology of HMs in the CPB, further investigations are necessary.

5. Conclusion

In this study, slag-based cementitious material was prepared using BFS, clinker, gypsum, and activator, to replace OPC in mine backfill pastes. To elucidate the influence of slag-based cementitious material on the behavior of CPB, the mechanical properties, toxicity leachability, chemical speciation of HMs, and microstructure evolution of CPB were explored using UCS, TCLP, BCR, SEM, XRD, FTIR, and MIP tests, respectively. A series of CPB samples with different slag-based cementitious material dosages (5%, 10%, 15%, and 20%) were prepared and cured for different durations (3, 7, 28, and 60 days). Based on the results of the above test, the major conclusions that could be drawn are:

1) The increase in binder dosage and curing time could effectively accelerate the activity of slag-based cementitious material and greatly enhance the compressive strength of the CPB. The UCS of sample S20 reached approximately 1.13 MPa, 1.74 MPa, 2.38 MPa, and 2.80 MPa after 3, 7, 28, and 60 days of curing, respectively, which increased by 59.15%, 64.15%, 64.14%, and 78.34% compared with that of sample C20 and therefore, met the requirements for backfill in mines.
2) The addition of slag-based cementitious material could decrease the leachate concentrations of Pb, Cr, Cu, and Cd in the CPB. The HMs that leached from the CPB specimens did not exceed the permissible limit. The exchangeable fraction content of Pb, Cr, Cu, and Cd was strongly correlated with binder dosage and curing time. When the slag-based cementitious material dosage and curing time was increased, the exchangeable fraction of HMs in the CPB decreased at different levels. It showed that HMs were stabilized using slag-based cementitious material, which reduced their harm to the environment.
3) The main hydration products of CPB were C–S–H gel, ettringite crystals, and portlandite. As the curing proceeded, the microstructure assumed a more compact network structure with lower porosity. The addition of slag-based cementitious material accelerated the hydration reaction with the generation of denser structures, leading to better mechanical strength and immobilization effect of the HMs.

Declarations

Author contribution statement

Fawen Zhang: Conceived and designed the experiments; Wrote the paper.

Yinyue Li; Jinhui Zhang: Performed the experiments.

Xin Gui; Xiuhong Zhu: Analyzed and interpreted the data.

Changmin Zhao: Contributed reagents, materials, analysis tools or data.

Funding statement

Ph.D. Fawen Zhang was supported by National Natural Science Foundation of China [51008118], Key Scientific Research Project of Henan Higher Education Institutions [18B610001], Science and Technology Innovation Foundation of Henan Agricultural University [KJCX2017A06].

Data availability statement

Data included in article/supp. material/referenced in article.

Declaration of interests statement

The authors declare no conflict of interest.

Additional information

No additional information is available for this paper.

References

[1] X. Kan, Y. Dong, L. Feng, M. Zhou, H. Hou, Contamination and health risk assessment of heavy metals in China's lead-zinc mine tailings: a meta-analysis, Chemosphere 267 (2021) 128909.
[2] C. Li, Q. Wen, M. Hong, Z. Liang, Z. Zhuang, Y. Yu, Heavy metals leaching in bricks made from lead and zinc mine tailings with varied chemical components, Construct. Build. Mater. 134 (2017) 443–451.
[3] Y. Zhang, W. Wu, Q. Liu, L. Sheng, Studying with small sample for leaching behavior of heavy metals based on the fuzzy theory, World J. Eng. 12 (3) (2015) 271–282.
[4] S. Zhang, Y. Zhao, Z. Guo, H. Ding, Stabilization/solidification of hexavalent chromium containing tailings using low-carbon binders for cemented paste backfill, J. Environ. Chem. Eng. 9 (1) (2021), 104738.
[5] A. Kesimal, B. Ercikdi, E. Yilmaz, The effect of desliming by sedimentation on paste backfill performance, Miner. Eng. 16 (10) (2003) 1009–1011.
[6] M. Fall, J.C. Célestin, F.S. Han, Suitability of bentonite-paste tailings mixtures as engineering barrier material for mine waste containment facilities, Miner. Eng. 22 (9) (2009) 840–848.
[7] J.L. Broadhurst, J.G. Petrie, Ranking and scoring potential environmental risks from solid mineral wastes, Miner. Eng. 23 (3) (2010) 182–191.
[8] C. Yue, Low-carbon binders produced from waste glass and low-purity metakaolin for cemented paste backfill, Construct. Build. Mater. 312 (2021), 125443.
[9] M. Fall, T. Belem, S. Samb, M. Benzaazoua, Experimental characterization of the stress-strain behaviour of cemented paste backfill in compression, J. Mater. Sci. 42 (11) (2007) 3914–3922.
[10] M. Fall, D. Adrien, J.C. Celestin, M. Pokharel, M. Toure, Saturated hydraulic conductivity of cemented paste backfill, Miner. Eng. 22 (15) (2009) 1307–1317.
[11] C. Qi, Q. Chen, A. Fourie, J. Zhao, Q. Zhang, Pressure drop in pipe flow of cemented paste backfill: experimental and modeling study, Powder Technol 333 (2018) 9–18.
[12] D. Ma, J. Zhang, H. Duan, Y. Huang, M. Li, Q. Sun, N. Zhou, Reutilization of gangue wastes in underground backfilling mining: overburden aquifer protection, Chemosphere 264 (2021), 128400.
[13] Q. Chen, Y. Tao, Q. Zhang, C. Qi, The rheological, mechanical and heavy metal leaching properties of cemented paste backfill under the influence of anionic polyacrylamide, Chemosphere 286 (Pt 1) (2022), 131630.
[14] A.J. Bull, M. Fall, Thermally induced changes in metalloid leachability of cemented paste backfill that contains blast furnace slag, Miner. Eng. 156 (2020), 106520.
[15] W. Li, M. Fall, Strength and self-desiccation of slag-cemented paste backfill at early ages: link to initial sulphate concentration, Cement Concr. Compos. 89 (2018) 160–168.
[16] E. Yilmaz, Stope depth effect on field behaviour and performance of cemented paste backfills, Int. J. Min. Reclamat. Environ. 32 (4) (2018) 273–296.
[17] C. Qi, A. Fourie, Cemented paste backfill for mineral tailings management: review and future perspectives, Miner. Eng. 144 (2019), 106025.
[18] M.T. Marvila, J. Alexandre, A.R.G. Azevedo, E.B. Zanelato, G.C. Xavier, S.N. Monteiro, Study on the replacement of the hydrated lime by kaolinitic clay in mortars, Adv. Appl. Ceram. 118 (7) (2019) 373–380.
[19] B.A. Tayeh, M.W. Hasaniyah, A.M. Zeyad, M.M. Awad, A. Alaskar, A.M. Mohamed, R. Alyousef, Durability and mechanical properties of seashell partially-replaced cement, J. Build. Eng. 31 (2020), 101328.
[20] L. Wang, S.S. Chen, D.C.W. Tsang, C. Poon, K. Shih, Recycling contaminated wood into eco-friendly particleboard using green cement and carbon dioxide curing, J. Clean. Prod. 137 (2016) 861–870.
[21] D.C. Vinh, S. Pilehvar, C. Salas-Bringas, A.M. Szczotok, N.B.D. Do, T.L. Hoa, M. Carmona, J.F. Rodriguez, A. Kjoniksen, Influence of microcapsule size and shell polarity on the time-dependent viscosity of geopolymer paste, Ind. Eng. Chem. Res. 57 (29) (2018) 9457–9464.
[22] J. Qiu, Y. Zhao, J. Xing, X. Sun, Fly ash/blast furnace slag-based geopolymer as a potential binder for mine backfilling: effect of binder type and activator concentration, Adv. Mater. Sci. Eng. 2019 (2019).
[23] Y. Zhao, J. Qiu, S. Zhang, Z. Guo, P. Wu, X. Sun, X. Gu, Low carbon binder modified by calcined quarry dust for cemented paste backfill and the associated environmental assessments, J. Environ. Manag. 300 (2021), 113760.
[24] X. Cheng, D. Long, C. Zhang, X. Gao, Y. Yu, K. Mei, C. Zhang, X. Guo, Z. Chen, Utilization of red mud, slag and waste drilling fluid for the synthesis of slag-red mud cementitious material, J. Clean. Prod. 238 (2019), 117902.
[25] A. Saedi, A. Jamshidi-Zanjani, A.K. Darban, A review on different methods of activating tailings to improve their cementitious property as cemented paste and reusability, J. Environ. Manag. 270 (2020), 110881.
[26] T. Yilmaz, B. Ercikdi, F. Cihangir, Evaluation of the neutralization performances of the industrial waste products (IWPs) in sulphide-rich environment of cemented paste backfill, J. Environ. Manag. 258 (2020).
[27] B. Ercikdi, F. Cihangir, A. Kesimal, H. Deveci, I. Alp, Utilization of industrial waste products as pozzolanic material in cemented paste backfill of high sulphide mill tailings, J. Hazard. Mater. 168 (2-3) (2009) 848–856.
[28] S.K. Behera, D.P. Mishra, P. Singh, K. Mishra, S.K. Mandal, C.N. Ghosh, R. Kumar, P.K. Mandal, Utilization of mill tailings, fly ash and slag as mine paste backfill material: review and future perspective, Construct. Build. Mater. 309 (2021), 125120.
[29] A. Fernandez, J.L. Garcia Calvo, M.C. Alonso, Ordinary Portland Cement composition for the optimization of the synergies of supplementary cementitious materials of ternary binders in hydration processes, Cement Concr. Compos. 89 (2018) 238–250.
[30] S. Zhang, L. Yang, F. Ren, J. Qiu, H. Ding, Rheological and mechanical properties of cemented foam backfill: effect of mineral admixture type and dosage, Cement Concr. Compos. 112 (2020), 103689.
[31] Q. Sun, S. Tian, Q. Sun, B. Li, C. Cai, Y. Xia, X. Wei, Q. Mu, Preparation and microstructure of fly ash geopolymer paste backfill material, J. Clean. Prod. 225 (2019) 376–390.
[32] Y. He, Q. Chen, C. Qi, Q. Zhang, C. Xiao, Lithium slag and fly ash-based binder for cemented fine tailings backfill, J. Environ. Manag. 248 (2019), 109282.
[33] X. Deng, J. Zhang, B. Klein, N. Zhou, B. DeWit, Experimental characterization of the influence of solid components on the rheological and mechanical properties of cemented paste backfill, Int. J. Miner. Process. 168 (2017) 116–125.
[34] Q. Chen, Y. Tao, Y. Feng, Q. Zhang, Y. Liu, Utilization of modified copper slag activated by Na2SO4 and CaO for unclassified lead/zinc mine tailings based cemented paste backfill, J. Environ. Manag. 290 (2021), 112608.
[35] H. Jiang, Z. Qi, E. Yilmaz, J. Han, J. Qiu, C. Dong, Effectiveness of alkali-activated slag as alternative binder on workability and early age compressive strength of cemented paste backfills, Construct. Build. Mater. 218 (2019) 689–700.
[36] J. Zheng, X. Sun, L. Guo, S. Zhang, J. Chen, Strength and hydration products of cemented paste backfill from sulphide-rich tailings using reactive MgO-activated slag as a binder, Construct. Build. Mater. 203 (2019) 111–119.
[37] J. Zheng, Y. Zhu, Z. Zhao, Utilization of limestone powder and water-reducing admixture in cemented paste backfill of coarse copper mine tailings, Construct. Build. Mater. 124 (2016) 31–36.
[38] H. Eker, A. Bascetin, Influence of silica fume on mechanical property of cemented paste backfill, Construct. Build. Mater. 317 (2022), 126089.
[39] J. Kiventerä, H. Sreenivasan, C. Cheeseman, P. Kinnunen, M. Illikainen, Immobilization of sulfates and heavy metals in gold mine tailings by sodium silicate and hydrated lime, J. Environ. Chem. Eng. 6 (5) (2018) 6530–6536.
[40] D. Zhao, Reactive MgO-modified slag-based binders for cemented paste backfill and potential heavy-metal leaching behavior, Construct. Build. Mater. 298 (2021), 123894.
[41] L. Wang, B. Ji, Y. Hu, R. Liu, W. Sun, A review on in situ phytoremediation of mine tailings, Chemosphere 184 (2017) 594–600.
[42] S. Hu, L. Zhong, X. Yang, H. Bai, B. Ren, Y. Zhao, W. Zhang, X. Ju, H. Wen, S. Mao, R. Tao, C. Li, Synthesis of rare earth tailing-based geopolymer for efficiently immobilizing heavy metals, Construct. Build. Mater. 254 (2020), 119273.
[43] R. Argane, M. Benzaazoua, R. Hakkou, A. Bouamrane, Reuse of base-metal tailings as aggregates for rendering mortars: assessment of immobilization performances and environmental behavior, Construct. Build. Mater. 96 (2015) 296–306.
[44] Y. Zhang, S. Zhang, W. Ni, Q. Yan, W. Gao, Y. Li, Immobilisation of high-arsenic-containing tailings by using metallurgical slag-cementing materials, Chemosphere 223 (2019) 117–123.
[45] Y. Zhang, W. Gao, W. Ni, S. Zhang, Y. Li, K. Wang, X. Huang, P. Fu, W. Hu, Influence of calcium hydroxide addition on arsenic leaching and solidification/stabilisation behaviour of metallurgical-slag-based green mining fill, J. Hazard. Mater. 390 (2020), 122161.

[46] Q. Wan, F. Rao, S. Song, Y. Zhang, Immobilization forms of ZnO in the solidification/stabilization (S/S) of a zinc mine tailing through geopolymerization, J. Mater. Res. Technol. 8 (6) (2019) 5728–5735.

[47] Q. Wan, F. Rao, S. Song, R. Morales-Estrella, X. Xie, X. Tong, Chemical forms of lead immobilization in alkali-activated binders based on mine tailings, Cement Concr. Compos. 92 (2018) 198–204.

[48] S. Dadsetan, J. Bai, Mechanical and microstructural properties of self-compacting concrete blended with metakaolin, ground granulated blast-furnace slag and fly ash, Construct. Build. Mater. 146 (2017) 658–667.

[49] J.F. López-Perales, J.E. Contreras, F.J. Vázquez-Rodríguez, C. Gómez-Rodríguez, L. Díaz-Tato, F. Banda-Muñoz, E.A. Rodríguez, Partial replacement of a traditional raw material by blast furnace slag in developing a sustainable conventional refractory castable of improved physical-mechanical properties, J. Clean. Prod. 306 (2021), 127266.

[50] G. Xue, E. Yilmaz, W. Song, S. Cao, Compressive strength characteristics of cemented tailings backfill with alkali-activated slag, Appl. Sci-Basel. 8 (9) (2018).

[51] S. Kumar, R. Kumar, A. Bandopadhyay, T.C. Alex, B. Ravi Kumar, S.K. Das, S.P. Mehrotra, Mechanical activation of granulated blast furnace slag and its effect on the properties and structure of portland slag cement, Cement Concr. Compos. 30 (8) (2008) 679–685.

[52] B. Xiao, Z. Wen, S. Miao, Q. Gao, Utilization of steel slag for cemented tailings backfill: hydration, strength, pore structure, and cost analysis, Case Stud. Constr. Mater. 15 (2021), e621.

[53] X. Chen, X. Shi, J. Zhou, X. Du, Q. Chen, X. Qiu, Effect of overflow tailings properties on cemented paste backfill, J. Environ. Manag. 235 (2019) 133–144.

[54] C. Chen, X. Li, X. Chen, J. Chai, H. Tian, Development of cemented paste backfill based on the addition of three mineral additions using the mixture design modeling approach, Construct. Build. Mater. 229 (2019), 116919.

[55] GB/T 1345-2005, The Test Sieving Method for Fineness of Cement, 2005.

[56] GB/T 1346-2011, Test Methods for Water Requirement of normal Consistency, Setting Time and Soundness of the portland Cement, 2012.

[57] GB/T 8074-2008, Testing Method for Specific Surface of Cement-Blaine Method, 2008.

[58] GB/T 17671-1999, Method of Testing Cements-Determination of Strength, 1999.

[59] ASTM C109/C109M-2016, Standard test method for compressive strength of hydraulic cement mortars (Using 2-in. Or [50-mm] Cube Specimens), 2016.

[60] F. Zhang, Y. He, C. Zhao, Y. Kou, K. Huang, Heavy metals pollution characteristics and health risk assessment of farmland soils and agricultural products in a mining area of Henan Province, China, Pol. J. Environ. Stud. 29 (5) (2020) 3929–3941.

[61] GB 15618-2018, Soil Environmental Quality-Risk Control Standard for Soil Contamination of Agricultural Land, 2018.

[62] GB 5085.3-2007, Identification Standards for Hazardous Wastes-Identification for Extraction Toxicity, 2007.

[63] F. Xue, T. Wang, M. Zhou, H. Hou, Self-solidification/stabilisation of electrolytic manganese residue: mechanistic insights, Construct. Build. Mater. 255 (2020), 118971.

[64] W. Li, Y. Sun, Y. Huang, T. Shimaoka, H. Wang, Y. Wang, L. Ma, D. Zhang, Evaluation of chemical speciation and environmental risk levels of heavy metals during varied acid corrosion conditions for raw and solidified/stabilized MSWI fly ash, Waste Manage 87 (2019) 407–416.

[65] Y. Feng, Y. Du, A. Zhou, M. Zhang, J. Li, S. Zhou, W. Xia, Geoenvironmental properties of industrially contaminated site soil solidified/stabilized with a sustainable by-product-based binder, Sci. Total Environ. 765 (2021), 142778.

[66] B. Ercikdi, H. Baki, M. İzki, Effect of desliming of sulphide-rich mill tailings on the long-term strength of cemented paste backfill, J. Environ. Manag. 115 (2013) 5–13.

[67] K. Klein, D. Simon, Effect of specimen composition on the strength development in cemented paste backfill, Can. Geotech. J. 43 (3) (2006) 310–324.

[68] W. Li, M. Fall, Sulphate effect on the early age strength and self-desiccation of cemented paste backfill, Construct. Build. Mater. 106 (2016) 296–304.

[69] M. Fall, M. Pokharel, Coupled effects of sulphate and temperature on the strength development of cemented tailings backfills: portland cement-paste backfill, Cement Concr. Compos. 32 (10) (2010) 819–828.

[70] A.J. Bull, M. Fall, Curing temperature dependency of the release of arsenic from cemented paste backfill made with Portland cement, J. Environ. Manag. 269 (2020), 110772.

[71] Q. Dong, B. Liang, L. Jia, L. Jiang, Effect of sulfide on the long-term strength of lead-zinc tailings cemented paste backfill, Construct. Build. Mater. 200 (2019) 436–446.

[72] X. Tian, F. Rao, C.A. León-Patiño, S. Song, Co-disposal of MSWI fly ash and spent caustic through alkaline-activation: immobilization of heavy metals and organics, Cement Concr. Compos. 114 (2020), 103824.

[73] Z. Gong, L. Liu, H. Zhang, Z. Wang, J. Wu, Y. Guo, J. Zhang, Study on migration characteristics of heavy metals during the oil sludge incineration with CaO additive, Chem. Eng. Res. Des. 166 (2021) 55–66.

[74] Y. Li, X. Min, L. Chai, M. Shi, C. Tang, Q. Wang, Y. Liang, J. Lei, W. Liyang, Co-treatment of gypsum sludge and Pb/Zn smelting slag for the solidification of sludge containing arsenic and heavy metals, J. Environ. Manag. 181 (2016) 756–761.

[75] T. Nakakubo, A. Tokai, K. Ohno, Comparative assessment of technological systems for recycling sludge and food waste aimed at greenhouse gas emissions reduction and phosphorus recovery, J. Clean. Prod. 32 (2012) 157–172.

[76] L. Liu, J. Xin, C. Qi, H. Jia, K. Song, Experimental investigation of mechanical, hydration, microstructure and electrical properties of cemented paste backfill, Construct. Build. Mater. 263 (2020).

[77] S. Chen, Z. Du, Z. Zhang, D. Yin, F. Feng, J. Ma, Effects of red mud additions on gangue-cemented paste backfill properties, Powder Technol 367 (2020) 833–840.

[78] L. Liu, Z. Fang, M. Wang, C. Qi, Y. Zhao, C. Huan, Experimental and numerical study on rheological properties of ice-containing cement paste backfill slurry, Powder Technol 370 (2020) 206–214.

[79] S. Chen, Z. Du, Z. Zhang, H. Zhang, Z. Xia, F. Feng, Effects of chloride on the early mechanical properties and microstructure of gangue-cemented paste backfill, Construct. Build. Mater. 235 (2020), 117504.

[80] L. Liu, J. Xin, C. Huan, C. Qi, W. Zhou, K. Song, Pore and strength characteristics of cemented paste backfill using sulphide tailings: effect of sulphur content, Construct. Build. Mater. 237 (2020), 117452.

[81] F. Cihangir, B. Ercikdi, A. Kesimal, S. Ocak, Y. Akyol, Effect of sodium-silicate activated slag at different silicate modulus on the strength and microstructural properties of full and coarse sulphidic tailings paste backfill, Construct. Build. Mater. 185 (2018) 555–566.

[82] J. Wang, X. Lyu, L. Wang, X. Cao, Q. Liu, H. Zang, Influence of the combination of calcium oxide and sodium carbonate on the hydration reactivity of alkali-activated slag binders, J. Clean. Prod. 171 (2018) 622–629.

[83] Y. Senhadji, G. Escadeillas, M. Mouli, H. Khelafi, Benosman, Influence of natural pozzolan, silica fume and limestone fine on strength, acid resistance and microstructure of mortar, Powder Technol 254 (2014) 314–323.

[84] S. Zhang, Y. Zhao, H. Ding, J. Qiu, C. Hou, Effect of sodium chloride concentration and pre-curing time on the properties of cemented paste backfill in a sub-zero environment, J. Clean. Prod. 283 (2021).

[85] S. Zhang, Y. Zhao, H. Ding, J. Qiu, Z. Guo, Recycling flue gas desulfurisation gypsum and phosphogypsum for cemented paste backfill and its acid resistance, Construct. Build. Mater. 275 (2021).

[86] E. Opiso, C. Tabelin, C. Maestre, J. Aseniero, I. Park, M. Villacorte-Tabelin, Synthesis and characterization of coal fly ash and palm oil fuel ash modified artisanal and small-scale gold mine (ASGM) tailings based geopolymer using sugar mill lime sludge as Ca-based activator, Heliyon 7 (2021), e06654.

[87] N. Koshy, K. Dondrob, L. Hu, Q. Wen, J. Meegoda, Synthesis and characterization of geopolymers derived from coal gangue, fly ash and red mud, Construct. Build. Mater. 206 (2019) 287–296.

[88] M. Wojdyr, Fityk: a general-purpose peak fitting program, J. Appl. Crystallogr. 43 (2010) 1126–1128.

[89] N. Zhou, J. Zhang, S. Ouyang, X. Deng, C. Dong, E. Du, Feasibility study and performance optimization of sand-based cemented paste backfill materials, J. Clean. Prod. 259 (2020), 120798.

[90] B. Guo, B. Liu, J. Yang, S. Zhang, The mechanisms of heavy metal immobilization by cementitious material treatments and thermal treatments: a review, J. Environ. Manag. 193 (2017) 410–422.

[91] H.Y. Poh, G.S. Ghataora, N. Ghazireh, Soil stabilization using basic oxygen steel slag fines, J. Mater. Civ. Eng. 18 (2) (2006) 229–240.

[92] R. Hamberg, C. Maurice, L. Alakangas, The use of low binder proportions in cemented paste backfill - effects on As-leaching, Miner. Eng. 78 (2015) 74–82.

[93] Y. Du, N. Jiang, S. Liu, F. Jin, D.N. Singh, A.J. Puppala, Engineering properties and microstructural characteristics of cement-stabilized zinc-contaminated kaolin, Can. Geotech. J. 51 (3) (2014) 289–302.

[94] M. Chrysochoou, D. Dermatas, Evaluation of ettringite and hydrocalumite formation for heavy metal immobilization: literature review and experimental study, J. Hazard. Mater. 136 (1) (2006) 20–33.